

Optics Letters

Component-wise testing of laser-written integrated coupled-mode beam splitters

JUN GUAN,^{1,3} ADRIAN J. MENSSEN,² XIANG LIU,¹ JINGYU WANG,¹ AND MARTIN J. BOOTH^{1,*} 

¹Department of Engineering Science, University of Oxford, Parks Road, Oxford, OX1 3PJ, UK

²Clarendon Laboratory, Department of Physics, University of Oxford, Oxford, OX1 3PU, UK

³e-mail: jun.guan@eng.ox.ac.uk

*Corresponding author: martin.booth@eng.ox.ac.uk

Received 21 March 2019; revised 8 May 2019; accepted 13 May 2019; posted 13 May 2019 (Doc. ID 362975); published 14 June 2019

Photonic integrated circuits (PICs) are important enabling technologies for the developments of areas such as quantum information processing (QIP). Coupled-mode integrated beam splitters (IBS) are widely used in many PICs, so direct and accurate testing of individual IBSs inside a PIC is increasingly desirable, as the development of PICs for QIP is scaled up. Here we demonstrate a solution for component-wise testing of coupled-mode IBSs without limitations on component location and PIC architectures. The method is based on the imaging of an individual IBS with a custom-built multifunctional adaptive optical microscope, combined with the calculation of its beam-splitting ratio through numerical modelling.

Published by The Optical Society under the terms of the [Creative Commons Attribution 4.0 License](https://creativecommons.org/licenses/by/4.0/). Further distribution of this work must maintain attribution to the author(s) and the published article's title, journal citation, and DOI.

<https://doi.org/10.1364/OL.44.003174>

Photonic integrated circuits (PICs) are important technologies for many application areas, especially the miniaturization and scalability of quantum information processing (QIP) [1]. Many photonic QIPs rely on PICs based on networked interferometers [1–19], in which integrated beam splitters (IBSs) are essential components. The directional coupler (DC) [1], a form of coupled-mode IBS, has lower loss [15] than the X coupler [16] and, hence, has been a common choice for beam splitting in quantum PICs [1–14]. The majority of these have been fabricated with femtosecond laser direct writing (FLDW) [2–14].

Accurate testing of the beam-splitting ratio of individual IBSs inside a PIC is an important part of the full characterization of a quantum PIC [15,19–22]. Testing is also indispensable for quality control during PIC production, as accuracy and repeatability of fabrication are often an issue [5,7,15,21,23]. Existing test methods [15–16,20] are restricted in their capabilities and are not generally applicable to large-scale PICs. The radiometric method [16] is only suitable for testing high-scattering-loss planar PICs, bearing in mind that low loss is desired for many PICs, especially those for quantum application [15,18,19].

The procedure-based methods [15,20] only work for reconfigurable networks and suffer from error accumulation and indistinguishability issues; more importantly, the complexity of the measurement procedures will grow very quickly with the scale of the PIC and eventually become practically unfeasible.

Methods for relaxing the fabrication tolerances of DCs in a PIC, such as the one proposed by Miller [21], in practice, will also lose their validity for larger-scale quantum PICs, because the involved additional circuit complexity not only will incur extra manufacture cost, but also critically increase the overall circuit loss, bearing in mind that low loss is critical in many quantum applications [15,18,19]. Quantum process tomography [22,24], with which the effective overall transformation of a quantum PIC can be recovered, will also become practically unworkable due to quickly growing resource costs as the scale of the PIC increases [23].

Therefore, a solution for accurately testing individual IBSs within a PIC in a deterministic and direct manner without limitations on component location and PIC architecture would greatly aid the scaling up of quantum PICs, on which the development of QIPs relies. To this end, we demonstrate a solution for a component-wise test of a coupled-mode IBS by first imaging the IBS under test with the third-harmonic generation (THG) module of a custom-built three-dimensional (3D) adaptive multifunctional microscope and measuring the waveguide projected refractive index change with its quantitative phase microscopy (QPM) module, then ascertaining its beam-splitting ratio with a numerical simulation model. The 3D THG imaging can be directly performed on any component or any part of it without limitations on component location and PIC architecture. It is deterministic, and direct and free from accumulation of systematic errors and can work with both planar and 3D PIC chips.

As shown in Fig. 1, the 3D adaptive multifunctional microscope consisted of briefly, a Cr:forsterite laser (pulse duration 65 fs, repetition rate 100 MHz, wavelength of 1235 nm), a two-axis galvanometer scanner, a deformable membrane mirror for aberration correction, 1.15 NA water immersion objective lens, and the piezo z-translation stage. THG emission was collected in the forward direction. Aberrations were corrected by sequentially adjusting the amplitudes of the Zernike

polynomial modes added to the deformable mirror, in order to maximize the total image intensity. When THG is in operation, the flip mirror (FM) is flipped down, while, in QPM mode, the FM is flipped up, and a green LED is inserted between the condenser and filter. The capability of THG microscopy on imaging photonic structures in glass has been demonstrated in previous reports such as Ref. [25].

To demonstrate the measurement accuracy of this method, we first showed that it can be used to determine accurately the beam-splitting ratios of 3D tritters (three-port coupled-mode IBSs) [5]. The beam-splitting ratio of a 3D tritter is highly sensitive to the relative position between its three coupling waveguides. Using the THG images, we determined that the effective waveguide positions had been affected by the directional quill effect [26], which has recently been shown to affect waveguides in this writing regime [27]. The adjustment of modelling parameters based on these observations yielded accurate splitting ratios. The method was further demonstrated with the direct couplers, which are the most common IBSs.

A set of 3D tritters, such as the one shown schematically in Fig. 2(a), were written in Corning EAGLE 2000 glass through FLDW. The femtosecond laser writing system composed a laser with 170 fs pulse duration, 1 MHz repetition rate, and 514 nm wavelength; a 0.5 NA objective lens with which the circularly-polarized beam was focused into a glass chip; and a three-axis translation stage that was used to transversely scan the chip relative to the focus. The 3D tritters were all written with the same writing parameters, pulse energy of 85 nJ, and scanning speed of 2 mm/s, which were chosen to balance between propagation loss, mode profile, and polarization independence.

The 3D tritters were designed in a way that the three waveguides were situated at the vertices of an isosceles triangle in the coupling region, where three waveguides were brought close for mode coupling; the triangle was formed by shifting the top waveguide downwards ΔY from an equilateral triangle with side length of 8 μm to compensate for the effect of the elongated waveguide shape, as shown in the cross-sectional THG image of a tritter at its coupling region in Fig. 2(b). The set of 3D tritters was fabricated with ΔY varying from 0.2 to 1.4 μm , with fixed coupling lengths of 4.2 mm. After fabrication, the cross sections of the tritters at the coupling region were imaged with the THG microscopy module of the custom-built 3D

adaptive multifunctional microscope. The projected refractive index change of the waveguides was measured with the QPM module through solving the transport-of-intensity equation (TIE) [28]. The QPM module was built in the multifunctional adaptive THG microscope, as shown in Fig. 1, to permit side-by-side measurements.

Using the measured relative position between the coupling waveguides and the refractive index change, we simulated the output splitting ratio of the tritters through solving the following coupled-mode equations for three waveguides [29]:

$$i\partial_z A_1 = \beta_1 A_1 + k_{12} A_2 + k_{13} A_3, \quad (1)$$

$$i\partial_z A_2 = k_{21} A_1 + \beta_2 A_2 + k_{23} A_3, \quad (2)$$

$$i\partial_z A_3 = k_{31} A_1 + k_{32} A_2 + \beta_3 A_3, \quad (3)$$

where $A_i(z)$ is the amplitude of the electrical field in waveguide i , which is a function of propagation length z along the waveguide; k_{ij} is the coupling coefficient between waveguide i and j ; β_i is the propagation constant of waveguide i . It is worth stressing that all the three waveguides are assumed here to be identical, bearing in mind that all the waveguides in this experiment were written with the same writing parameters. It was assumed that the quill effect only effectively shifted the position of a waveguide [27]. The general solution of this equation system is given by

$$\vec{A}(z) = \vec{A}(0) \exp(-i\hat{K} \cdot z), \quad (4)$$

where \hat{K} is a matrix containing the coupling coefficients k_{ij} . The optical mode of the waveguides was calculated through numerically solving Maxwell's equations, with an input of the waveguide geometrical profile from the THG image and refractive index change from TIE microscopy. The coupling coefficient between two waveguides i and j can then be approximated by

$$k_{ij} \approx \frac{2\pi}{\lambda\beta_i} \int (n_j^2 - n^2) \Psi_i \Psi_j^* dA, \quad (5)$$

where n_j is the refractive index of waveguide, which is assumed to be the same for all waveguides written with the same writing parameters; n is the refractive index of waveguide surrounding material; the propagation constant β was assumed to be the

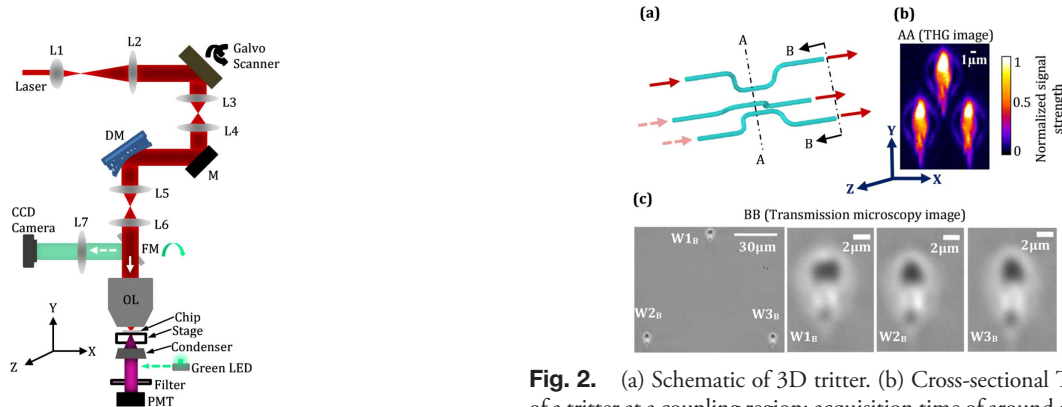


Fig. 1. Schematic of the custom-built 3D adaptive multifunctional microscope. L1–L7, lenses; M, mirror; DM, deformable mirror; FM, flip mirror; OL, objective lens; PMT, photomultiplier tube. QPM could be performed after inserting the green LED and flipping up the FM.

Fig. 2. (a) Schematic of 3D tritter. (b) Cross-sectional THG image of a tritter at a coupling region; acquisition time of around one minute. (c) Transmission cross-sectional image of a tritter taken with a transmission microscope (Zeiss Axioplan 2) at the chip end facet [position BB in (a)]. From left to right, the second to fourth pictures are the close-up images of waveguides on the first picture.

same for all waveguides; Ψ_i and Ψ_j are normalized near-field modes. For accurate simulation of the beam-splitting ratio, we determined the coupling coefficients k_{ij} , as well as the propagation constant β , based on a finite-element simulation in COMSOL.

Then the simulation model was calibrated with the measurement results of several fabricated 3D tritters, together with their determined waveguide relative positions in a coupling region based on THG images (detailed in the following text), during which a calibration constant was found. Then the constant was kept unchanged during simulation of all of the tritters and DCs.

The beam-splitting ratios of the 3D tritters and DCs were measured through butt-coupling laser beam from a polarization-maintaining fiber-coupled laser (Thorlabs S1FC780PM) through a polarization-maintaining fiber (Thorlabs P1-630PM-FC-5) at vertical polarization. The laser polarization direction was aligned along the waveguide transverse elongation direction, which was a birefringence axis of the waveguides. The output was coupled through an objective lens and measured with a photodiode power sensor.

According to the tritter design, the light-guiding centers of the three waveguides in coupling regions should be equidistant in the X direction, which meant the ratio of X_{12}/X_{13} in Fig. 3(a) should be unity but, after fabrication and analysis of the THG images, it was found out that for all the fabricated tritters the ratio of X_{12}/X_{13} was repeatable around 0.87. As shown in our previous report [27], this is due to the quill laser writing effect [26] since, within each tritter, waveguides W1 and W2 were fabricated with a scan direction opposite that of waveguide W3. The quill effect caused a shift in position

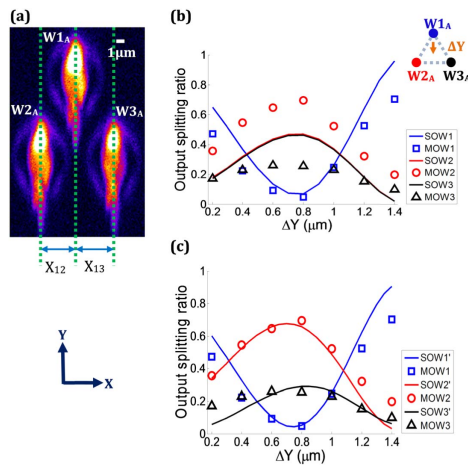


Fig. 3. Determining beam-splitting ratios of 3D tritters based on their THG images. (a) Cross-sectional THG image of a tritter at its coupling region. X_{12} is the distance in the X direction between the light-guiding centers of waveguide $W1_A$ and $W2_A$; X_{13} is the distance between $W1_A$ and $W3_A$; the scan direction during fabrication of waveguide $W1_A$ and $W2_A$ was opposite that of waveguide $W3_A$. (b) Measured beam-splitting ratios of the tritters and their simulated results based on the designed values of X_{12}/X_{13} ; in the legend, SOW1, 2 and 3 are simulated output beam-splitting ratios of waveguide port 1, 2, and 3, respectively; MOW1, 2, and 3 are the measured values; in the inset is schematic of tritter at coupling region (c) Measured beam-splitting ratios (MOW1, 2, and 3) of the tritters and their simulated results (SOW1, 2', and 3') based on the X_{12}/X_{13} value determined from THG images.

of the waveguide's light-guiding center [27]. The simulated output beam-splitting ratios of the tritters based on the designed and ascertained X_{12}/X_{13} values from the THG images were both compared with the measured beam-splitting ratios, as shown in Figs. 3(b) and 3(c), respectively. It can be clearly seen that the simulated results based on the X_{12}/X_{13} value determined with the THG images agreed well with the measured values, but the simulated results based on the designed value of X_{12}/X_{13} did not.

The subtle discrepancy between the designed and measured X_{12}/X_{13} values cannot be detected in a non-destructive manner using conventional microscopes that lack the 3D resolution of the THG microscope. This would be even more challenging in a multiple-component PIC chip, where different IBSs could lie adjacent to or above each other. While cross-sectional images of the end facets [Fig. 2(c)] are possible, these would not reveal the necessary information of the waveguides in the coupling region.

The DC is a widely used component that is simpler in form than the tritter, as shown in Figs. 4(a) and 4(b). We demonstrated the new characterization method on a set of DCs that were fabricated with the same writing parameters as those for the tritters. The DCs were designed with a separation of 8 μm between two waveguides in the coupling regions (referred to for brevity as "separation" hereafter). The coupling length C varied from 1.6 to 4.4 mm with increments of 0.2 mm. To compare the influence of the quill effect on tritter and DC, the DC waveguides were also written with opposite scan directions. Between the tritter and the DC, the only change to the numerical simulation model was the reduction of the number of coupled waveguides in Eqs. (1)–(3) to two; other parameters were kept unchanged. The simulated output beam-splitting ratios based on the designed separation value and those based on separation determined with THG images are compared with the actual measurement results through light coupling-in measurement, as shown in Fig. 4(c). We can see that the simulated

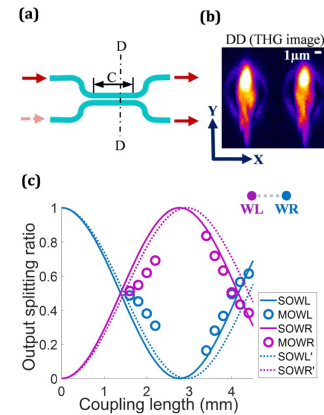


Fig. 4. Determining beam-splitting ratios of DCs based on their THG images. (a) Schematic of DC; C denotes the coupling length. (b) Cross-sectional THG image of a DC at its coupling region. (c) Measured and simulated output splitting ratios of DCs aiming at 41% and 50% reflectivity; in the inset is the schematic of the two waveguides (WL and WR) in the coupling region; in the legend, SOWL and SOWR are simulated beam-splitting ratios of the waveguide WL and WR, respectively, based on designed separation; SOWL' and SOWR' are the simulated beam-splitting ratios based on separation decided from the THG image; MOWL and MOWR are the measured beam-splitting ratios.

results agree reasonably well with the actual measurement results, considering that the simulation model was calibrated with the tritters, not the DCs. From Fig. 4(c), we can see that in the tested coupling length range the difference between simulated results based on designed separation and those based on separation determined from THG image was not as big as that with tritters. The reasons for that are as follows: (1) in principle, the DC is less sensitive to the deviation of separation than tritter; (2) we found that with the same fabrication parameters and being fabricated on the same chip, the shift of the relative position in the X direction between the waveguide light-guiding centers of a DC, resulting from the quill effect, was significantly smaller than that of a tritter. Therefore, after comparing the THG images shown in Figs. 3(a) and 4(b), we suspect that the impact of the quill effect on the shift of the waveguide guiding center depends not only on fabrication parameters and substrate material, but also on the separation and orientation between a newly written waveguide and nearby existing waveguides.

Limited by available computing power, we developed the simulation model based on a coupled-mode theory, which can be run on a normal personal computer, but cannot be used to simulate polarization related properties. Thus, all the beam-splitting ratio measurement results in this experiment were measured with a vertically polarized laser whose polarization direction was aligned along the waveguide transverse elongation direction, which was a birefringence axis of the waveguides, to avoid the influence of polarization. The method could be straightforwardly upgraded to be polarization-compatible by simulating the IBSs with a 3D Maxwell's solver, after input of the complete 3D waveguides profiles from THG imaging (as exemplified in Visualization 1). Then the phase difference between ports of an IBS could also be determined. The simulation accuracy could also be improved, above the current 8% and 12% standard deviations between measurement and simulation results for tritter and DC, respectively. Although this method was demonstrated for FLDW-PICs in glass, we expect this solution can be used for component-wise testing of any silica-on-silicon coupled-mode IBS such as those fabricated with a standard complementary metal-oxide-semiconductor process [17,18].

In summary, based on adaptive 3D multimodal microscopy, we demonstrated a solution for component-wise testing of the beam-splitting ratio of a coupled-mode IBS, the prevalent type of IBS, in a direct and deterministic manner without limitations on component location and PIC architecture. Moreover, unlike the existing methods [15–16,20] and the component-wise test methods for other applications [30–32], this solution does not require excitation of the device under inspection. It can be used not only for quality control during PIC production, but also for PIC characterization for high-demand applications such as the faithful execution of QIP protocols. From a testing perspective, it facilitates further up-scaling of PICs, especially for quantum applications.

Funding. Engineering and Physical Sciences Research Council (EPSRC) (EP/K034480/1, EP/M013243/1).

REFERENCES

1. A. Politi, M. J. Cryan, J. G. Rarity, S. Yu, and J. L. O'Brien, *Science* **320**, 646 (2008).
2. L. Sansoni, F. Sciarrino, G. Vallone, P. Mataloni, A. Crespi, R. Ramponi, and R. Osellame, *Phys. Rev. Lett.* **105**, 200503 (2010).
3. A. Crespi, R. Ramponi, R. Osellame, L. Sansoni, I. Bongioanni, F. Sciarrino, G. Vallone, and P. Mataloni, *Nat. Commun.* **2**, 566 (2011).
4. L. Sansoni, F. Sciarrino, G. Vallone, P. Mataloni, A. Crespi, R. Ramponi, and R. Osellame, *Phys. Rev. Lett.* **108**, 010502 (2012).
5. N. Spagnolo, C. Vitelli, L. Aparo, P. Mataloni, F. Sciarrino, A. Crespi, R. Ramponi, and R. Osellame, *Nat. Commun.* **4**, 1606 (2013).
6. A. Crespi, R. Osellame, R. Ramponi, V. Giovannetti, R. Fazio, L. Sansoni, F. De Nicola, F. Sciarrino, and P. Mataloni, *Nat. Photonics* **7**, 322 (2013).
7. M. Tillmann, B. Dakić, R. Heilmann, S. Nolte, A. Szameit, and P. Walther, *Nat. Photonics* **7**, 540 (2013).
8. T. Meany, M. Gräfe, R. Heilmann, A. Perez-Leija, S. Gross, M. J. Steel, M. J. Withford, and A. Szameit, *Laser Photonics Rev.* **9**, 363 (2015).
9. Z. Chaboyer, T. Meany, L. G. Helt, M. J. Withford, and M. J. Steel, *Sci. Rep.* **5**, 9601 (2015).
10. T. Meany, D. N. Biggerstaff, M. A. Broome, A. Fedrizzi, M. Delanty, M. J. Steel, A. Gilchrist, G. D. Marshall, A. G. White, and M. J. Withford, *Sci. Rep.* **6**, 25126 (2016).
11. M. A. Ciampini, A. Orioux, S. Paesani, F. Sciarrino, G. Corielli, A. Crespi, R. Ramponi, R. Osellame, and P. Mataloni, *Light Sci. Appl.* **5**, e16064 (2016).
12. I. Pitsios, L. Banchi, A. S. Rab, M. Bentivegna, D. Caprara, A. Crespi, N. Spagnolo, S. Bose, P. Mataloni, R. Osellame, and F. Sciarrino, *Nat. Commun.* **8**, 1569 (2017).
13. J. Zeuner, A. N. Sharma, M. Tillmann, R. Heilmann, M. Gräfe, A. Moqanaki, A. Szameit, and P. Walther, *NPJ Quantum Inf.* **4**, 13 (2018).
14. T. Giordani, F. Flamini, M. Pompili, N. Viggianiello, N. Spagnolo, A. Crespi, R. Osellame, N. Wiebe, M. Walschaers, A. Buchleitner, and F. Sciarrino, *Nat. Photonics* **12**, 173 (2018).
15. J. Mower, N. C. Harris, G. R. Steinbrecher, Y. Lahini, and D. Englund, *Phys. Rev. A* **92**, 032322 (2015).
16. B. J. Metcalf, N. Thomas-Peter, J. B. Spring, D. Kundys, M. A. Broome, P. C. Humphreys, X.-M. Jin, M. Barbieri, W. Steven Kolthammer, J. C. Gates, B. J. Smith, N. K. Langford, P. G. R. Smith, and I. A. Walmsley, *Nat. Commun.* **4**, 1356 (2013).
17. J. Carolan, C. Harrold, C. Sparrow, E. Martín-López, N. J. Russell, J. W. Silverstone, P. J. Shadbolt, N. Matsuda, M. Oguma, M. Itoh, G. D. Marshall, M. G. Thompson, J. C. F. Matthews, T. Hashimoto, J. L. O'Brien, and A. Laing, *Science* **349**, 711 (2015).
18. C. Sparrow, E. Martín-López, N. Maraviglia, A. Neville, C. Harrold, J. Carolan, Y. N. Joglekar, T. Hashimoto, N. Matsuda, J. L. O'Brien, D. P. Tew, and A. Laing, *Nature* **557**, 660 (2018).
19. B. J. Metcalf, J. B. Spring, P. C. Humphreys, N. Thomas-Peter, M. Barbieri, W. S. Kolthammer, X.-M. Jin, N. K. Langford, D. Kundys, J. C. Gates, B. J. Smith, P. G. R. Smith, and I. A. Walmsley, *Nat. Photonics* **8**, 770 (2014).
20. W. R. Clements, P. C. Humphreys, B. J. Metcalf, W. S. Kolthammer, and I. A. Walmsley, *Optica* **3**, 1460 (2016).
21. D. A. B. Miller, *Optica* **2**, 747 (2015).
22. M. Lobino, D. Korystov, C. Kupchak, E. Figueroa, B. C. Sanders, and A. I. Lvovsky, *Science* **322**, 563 (2008).
23. T. Max, S. Christian, and W. Philip, *J. Opt.* **18**, 114002 (2016).
24. M. W. Mitchell, C. W. Ellenor, S. Schneider, and A. M. Steinberg, *Phys. Rev. Lett.* **91**, 120402 (2003).
25. J. Guan, X. Liu, and M. J. Booth, *Opt. Lett.* **44**, 1039 (2019).
26. P. G. Kazansky, W. Yang, E. Bricchi, J. Bovatsek, A. Arai, Y. Shimotsuma, K. Miura, and K. Hirao, *Appl. Phys. Lett.* **90**, 151120 (2007).
27. J. Guan, X. Liu, and M. J. Booth, *Opt. Express* **26**, 30716 (2018).
28. A. Jesacher, P. S. Salter, and M. J. Booth, *Opt. Mater. Express* **3**, 1223 (2013).
29. W.-P. Huang, *J. Opt. Soc. Am. A* **11**, 963 (1994).
30. N. Rotenberg and L. Kuipers, *Nat. Photonics* **8**, 919 (2014).
31. R. Bruck, B. Mills, B. Troia, D. J. Thomson, F. Y. Gardes, Y. Hu, G. Z. Mashanovich, V. M. N. Passaro, G. T. Reed, and O. L. Muskens, *Nat. Photonics* **9**, 54 (2014).
32. K. Vynck, N. J. Dinsdale, B. Chen, R. Bruck, A. Z. Khokhar, S. A. Reynolds, L. Cradginton, D. J. Thomson, G. T. Reed, P. Lalanne, and O. L. Muskens, *Nat. Commun.* **9**, 2246 (2018).